Bioconjugate Chemistry

Article

pubs.acs.org/bc

EGF Receptor-Targeting Peptide Conjugate Incorporating a Near-IR Fluorescent Dye and a Novel 1,4,7-Triazacyclononane-Based ^{64}Cu(II) Chelator Assembled via Click Chemistry

Katrin Viehweger,*[,†] Lisa Barbaro,[‖] Karina Pombo García,[†] Tanmaya Joshi,[⊥] Gerhard Geipel,[‡] Jörg Steinbach,[†,§] Holger Stephan,*[,†] Leone Spiccia,*[,⊥] and Bim Graham*[,‖]

[†]Institute of Radiopharmaceutical Cancer Research and [‡]Institute of Resource Ecology, Helmholtz-Zentrum Dresden-Rossendorf eV, P.O. Box 510119, D-01314 Dresden, Germany

[§]Technische Universität Dresden, Department of Chemistry and Food Chemistry, D-01062 Dresden, Germany

[‖]Monash Institute of Pharmaceutical Sciences, Monash University, Parkville, VIC 3052, Australia

[⊥]School of Chemistry, Monash University, Clayton, Vic 3800, Melbourne, Australia

Supporting Information

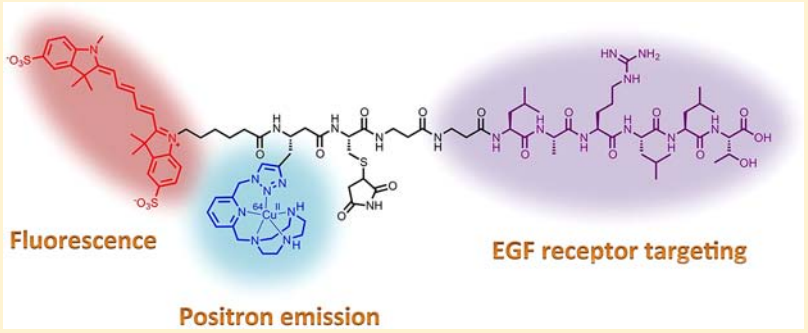

ABSTRACT: A new Boc-protected 1,4,7-triazacyclononane (TACN)-based pro-chelator compound featuring a "clickable" azidomethylpyridine pendant has been developed as a building block for the construction of multimodal imaging agents. Conjugation to a model alkyne (propargyl alcohol), followed by deprotection, generates a pentadentate ligand, as confirmed by X-ray crystallographic analysis of the corresponding distorted square-pyramidal Cu(II) complex. The ligand exhibits rapid ^{64}Cu(II)-binding kinetics (>95% radiochemical yield in <5 min) and a high resistance to demetalation. It may thus prove suitable for use in ^{64}Cu(II)-based *in vivo* positron emission tomography (PET). The new chelating building block has been applied to the construction of a bimodal (PET/fluorescence) peptide-based imaging probe targeting the epidermal growth factor (EGF) receptor, which is highly overexpressed on the surface of several types of cancer cells. The probe consists of a hexapeptide sequence, Leu-Ala-Arg-Leu-Leu-Thr (designated "D4"), followed by a Cys-β-Ala-β-Ala spacer, then a β-homopropargylglycine residue with the TACN-based chelator "clicked" to its side chain. A sulfonated near-infrared (NIR) fluorescent cyanine dye (sulfo-Cy5) was introduced at the N-terminus to study the EGF receptor-binding ability of the probe by laser-fluorescence spectroscopy. Binding was also confirmed by coimmunoprecipitation methods, and an apparent dissociation constant (K_d) of ca. 10 nM was determined from radioactivity-based measurements of probe binding to two EGF receptor-expressing cell lines (FaDu and A431). The probe is shown to be a biased or partial allosteric agonist of the EGF receptor, inducing phosphorylation of Thr669 and Tyr992, but not the Tyr845, Tyr998, Tyr1045, Tyr1068, or Tyr1148 residues of the receptor, in the absence of the orthosteric EGF ligand. Additionally, the probe was found to suppress the EGF-stimulated autophosphorylation of these latter residues, indicating that it is also a noncompetitive antagonist.

INTRODUCTION

Modern day diagnosis and treatment of cancer (as well as several other major diseases) is greatly assisted by a range of different molecular imaging techniques, including positron emission tomography (PET), single-photon emission computed tomography (SPECT), magnetic resonance imaging (MRI), and fluorescent optical imaging. However, because of inherent limitations in sensitivity, spatial and/or temporal resolution, and/or tissue penetrability, no method is sufficient on its own to gain full insight into tumor structure and pathology *in vivo*. Multimodal imaging is a relatively recent development that seeks to integrate the strengths of several imaging methods by employing hybrid scanners to produce separate images of a subject in one sitting; these are

Received: March 28, 2014
Revised: April 18, 2014
Published: April 22, 2014

 © 2014 American Chemical Society dx.doi.org/10.1021/bc5001388 | *Bioconjugate Chem.* 2014, 25, 1011−1022

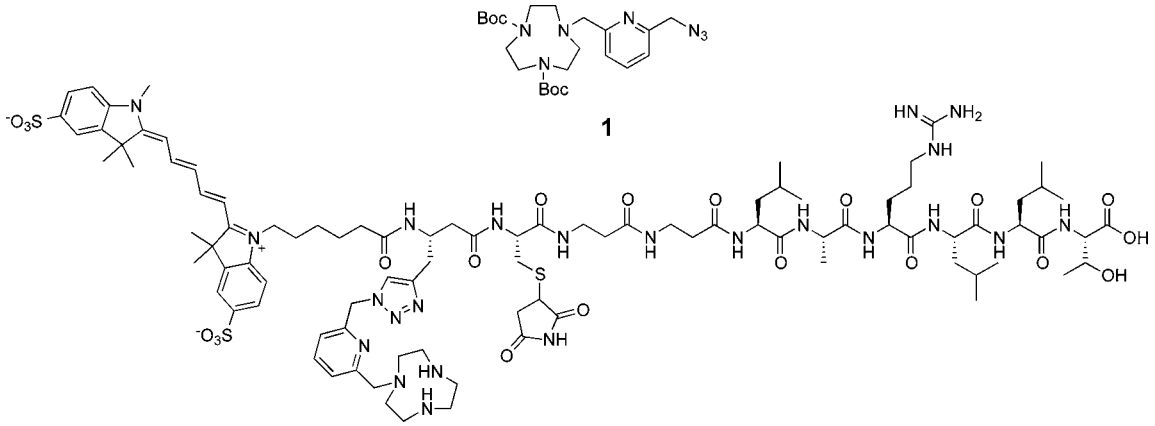

Figure 1. Structure of the "clickable" pro-chelator building block, **1**, and the EGF receptor-targeting peptide conjugate.

subsequently integrated through software to give an overlaid image.[1] In an effort to further enhance the quality of the data delivered through hybrid scanner technology, current research has focused heavily on the development of bi- and trimodal imaging probes.[2] The integration of more than one detectable moiety into a single imaging agent enables the efficient acquisition of data and ensures exact signal colocalization and pharmacokinetics, while also providing a less invasive alternative for the patient.

As part of our efforts to develop new multimodal imaging probes, we have sought to produce new ^{64}Cu(II)-chelating moieties that may be readily incorporated into peptide-based probe designs to allow for detection by PET. ^{64}Cu is a highly useful positron-emitting radiotracer because of its intermediate decay half-life of 12.7 h. Additionally, it and its "sister" radioisotope, ^{67}Cu, are promising agents for cancer imaging and radiotherapy.[3−11] For such applications, it is mandatory to incorporate the ^{64}Cu in the form of a highly stable complex. Among the diverse set of Cu(II)-binding bifunctional chelator systems reported,[12−16] we have developed promising platforms based on bispidine[17,18] and 1,4,7-triazacyclononane (TACN).[19−22] Here, we report a new TACN-based pro-chelator building block (Figure 1) that may be incorporated into multimodal imaging probe designs via the Cu(I)-catalyzed azide−alkyne cycloaddition reaction ("click chemistry").[23−32] Because of the "bio-orthogonal" nature of click chemistry, we envisage that this building block will prove useful for multimodal probe construction, helping obviate the need for protracted protection/deprotection schemes often encountered when only amide bond-forming reactions are employed.

In this study, the pro-chelator building block has been applied in the construction of a new bimodal imaging agent designed to target the epidermal growth factor (EGF) receptor. The EGF receptor is a cell-surface receptor whose over-expression and mutations are involved in carcinogenesis and the progression of many human cancers, including breast, lung, esophageal, head, and neck cancers.[33−36] Signaling of the receptor promotes proliferation, tumor cell motility, and angiogenesis, at the same time delaying apoptosis.

Several different strategies have been successfully developed to target the EGF receptor, with many of these comprehensively reviewed by Master and Gupta.[37] The targeting moieties reported to date include: (1) epidermal growth factor (EGF), a 6.2 kDa peptide[38] that is one of the native ligands of the EGF receptor;[39] (2) Cetuximab (C225), an anti-EGF receptor antibody, approved by the Food and Drug Administration (FDA) for the treatment of several cancers;[40,41] (3) single-chain anti-EGF receptor antibodies (ScFvEGFR);[42] (4) EGF receptor-binding affibodies based on a protein domain derived from one of the IgG-binding domains of *Staphylococcal* protein A;[43,44] (5) EGF receptor-binding nanobodies based on various domains of camelid heavy chain-only antibodies;[45−53] (6) small synthetic peptide sequences that bind specifically to the EGF receptor.[54−58]

Of these, small peptides are particularly attractive because they exhibit fast diffusion rates and low immunogenicity compared to antibodies and other proteins. In addition, they may be easily conjugated to, for example, nanoparticle-based drug delivery systems. Various EGF receptor-targeting peptides have been identified by phage display techniques or by computer-assisted design (CAD). The most studied of these are "D4" (LARLLT)[55] and "GE11" (YHWYGYTPQNVI),[54] both of which bind to the extracellular domain of the EGF receptor—GE11 to the binding pocket of the endogenous ligand[54] and D4 to a highly solvent-exposed region distinct from the EGF-binding site.[55]

Our new probe (Figure 1) consists of the D4 peptide coupled to a sulfonated near-infrared fluorescent cyanine dye ("sulfo-Cy5") via a *β*-homopropargylglycine-Cys-*β*-Ala-*β*-Ala spacer at its N-terminus. Additionally, the probe features a ^{64}Cu(II)-chelating moiety introduced by clicking our pro-chelator to the alkyne-bearing side chain of the *β*-homopropargylglycine residue. The cysteine residue was incorporated to allow for subsequent conjugation of multiple copies of the peptide to either a polymer or nanoparticle. For the purposes of this study, however, this residue was capped with maleimide so that the targeting properties of the peptide could be studied without complications arising from the reactivity of the cysteine thiol group. In addition to its assembly, the results of a study examining the EGF receptor binding ability of the probe are presented, which were performed as a prelude to the future development of more complex nanoparticle-based multimodal imaging agents.

RESULTS AND DISCUSSION

Synthesis and Preliminary Testing of the TACN-Based Pro-Chelator. The synthesis of the new pro-chelator building block (**1**) was achieved by a one-pot reaction involving azide substitution of one bromo group in 2,6-*bis*(bromomethyl)-pyridine using NaN_3, followed by substitution of the second bromo group by the secondary nitrogen present in di-*tert*-butyl-1,4,7-triazacyclononane-1,4-dicarboxylate (Boc_2TACN)

dx.doi.org/10.1021/bc5001388 | *Bioconjugate Chem.* 2014, 25, 1011−1022

(Scheme 1). This one-pot procedure was employed due to difficulties encountered in attempting to separate the initial

Scheme 1. Synthesis of the Pro-Chelator, 1[a]

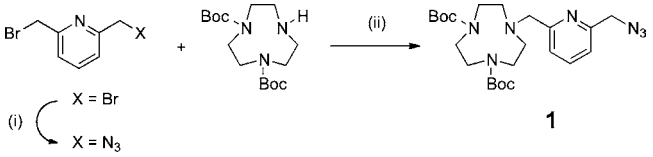

[a]Reagents and conditions: (i) NaN_3, CH_3CN, 60 °C, O/N; (ii) K_2CO_3, CH_3CN, reflux, O/N.

monoazide intermediate from the 2,6-*bis*(azidomethyl)pyridine that inevitably formed during the reaction. It was important to add sufficient NaN_3 to ensure maximum conversion of the 2,6-*bis*(bromomethyl)pyridine to a mixture of the mono- and diazide derivatives (as monitored by analytical HPLC), otherwise the unreacted dibromo compound coupled with Boc_2TACN in the subsequent step to produce a bridged *bis*(TACN) side-product that was difficult to separate from **1**.

We anticipated that upon "clicking" to a targeting vector, compound **1** would generate a pentadentate ligand capable of forming a square-pyramidal (SP) complex with a $^{64}Cu^{2+}$ ion, similar to that reported for our earlier TACN-based chelator, 1,4-*bis*(2-pyridylmethyl)-1,4,7-triazacyclononane (dmpTACN).[19,21] To confirm this, a model "click" reaction was carried out in which compound **3** was produced via a Cu(I)-catalyzed reaction between **1** and propargyl alcohol, using *tris*(hydroxypropyl-triazolylmethyl)amine (THPTA) as a Cu(I)-stabilizing ligand, followed by Boc deprotection (Scheme 2). The reaction proceeded rapidly (<1 h) and cleanly to give **2** in 92% yield. Subsequent TFA-mediated Boc deprotection gave **3** (as the TFA salt) in quantitative yield.

Single crystals of the Cu(II) complex of **3** (**C1·H_2O**) were grown by slowly diffusing Et_2O into a mixture of $CuCl_2$, **3**, and excess $NaClO_4$ dissolved in MeOH. The crystal structure consists of discrete mononuclear $[Cu(II)\text{-}3]^{2+}$ cations (Figure 2), perchlorate anions, and waters of crystallization. As predicted, the new ligand forms a distorted SP, 5-coordinate Cu(II) complex, with the metal center bound by all three TACN nitrogens, the pyridyl nitrogen and the triazole nitrogen in the 2 position (selected bond lengths and angles, together with crystal data and details of data collection, are provided in the Supporting Information). The apical site is occupied by the secondary TACN nitrogen and the bond between this atom and the Cu(II) center is longer (2.188(3) Å) than those within the basal plane (1.981(3)−2.031(3) Å) due to Jahn−Teller distortion imposed by the d^9 Cu^{2+} ion. The degree of distortion (τ) from ideal SP geometry toward trigonal bipyramidal (TBP) geometry can be defined as a function of the two largest basal angles, θ and Φ: $\tau = [(\theta - \Phi)/60)] \times 100$, with τ = 0% for an ideal SP and 100% for ideal TBP geometry.[59] The calculated τ

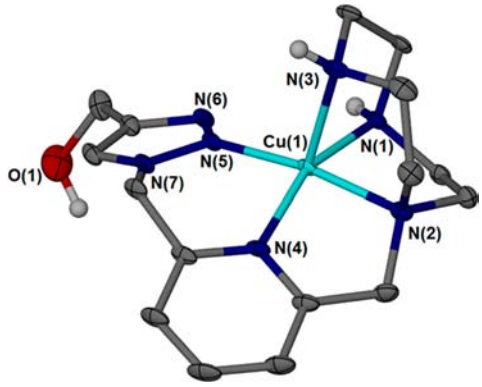

Figure 2. Thermal ellipsoid representation of cationic unit present in the crystal lattice of **C1·H_2O** (ellipsoids drawn at 30% probability; selected hydrogen atoms, noncoordinating water molecules, perchlorate counteranions, and the Cu(2) cationic unit containing disorder around the hydroxymethyl group have been omitted for clarity).

value of 8% indicates a copper(II) geometry close to regular SP. The distortion is largely associated with the constraints imposed by three edge-sharing, five-membered chelate rings of the TACN moiety, evidenced by the fact that within these chelate rings, the N−Cu−N angles (83−86°) are all below the 90° expected for an idealized SP structure.[60] The electronic spectrum of the crystals dissolved in aqueous solution exhibits a broad d-d transition centered at 580 nm, indicating that the SP coordination geometry observed in the crystalline state is maintained in solution.[59,60]

Treatment of **3** with $^{64}Cu^{2+}$ ions at 25 °C and pH 5.5 in 0.1 M 2-(*N*-morpholino)ethanesulfonic acid (MES) buffer was found to lead to extremely rapid formation (<5 min) of the corresponding ^{64}Cu(II) complex (Figure 3), with both radio-

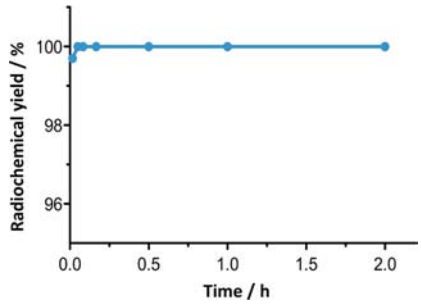

Figure 3. Kinetics of ^{64}Cu(II)-binding to **3** at 25 °C and pH 5.5 (0.1 MES buffer), as determined by radio-TLC analysis.

HPLC and radio-TLC exhibiting a single peak corresponding to the ^{64}Cu(II) complex of **3**, and no trace of free $^{64}Cu^{2+}$ ions (Figure S1). Competition ("challenge") experiments with the well-established Cu(II) chelator, 1,4,8,11-tetraazacyclotetrade-

Scheme 2. Synthesis of the Model Ligand, 3, by a Copper(I)-Catalyzed "Click" Reaction[a]

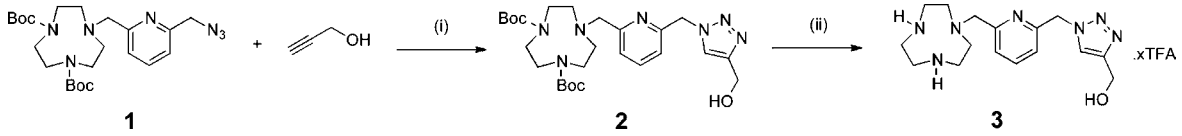

[a]Reagents and conditions: (i) $CuSO_4$, THPTA, sodium ascorbate, MeOH, RT, 1 h. (ii) TFA, DCM, RT, O/N.

dx.doi.org/10.1021/bc5001388 | *Bioconjugate Chem.* 2014, 25, 1011−1022

Scheme 3. Synthesis of Amino Acid Building Block 4 via a Copper(I)-Catalyzed "Click" Reaction between 1 and Fmoc-L-β-Homopropargylglycine[a]

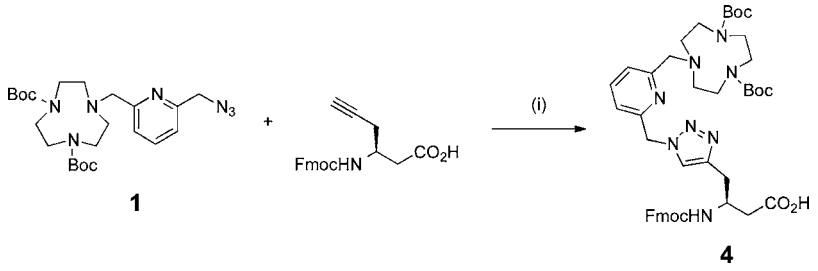

[a]Reagents and conditions: (i) $CuSO_4$, THPTA, sodium ascorbate, MeOH, MW 100 °C, 10 min.

cane-1,4,8,11-tetraacetic acid (TETA), indicated that the ^{64}Cu(II) complex was of high stability. Minimal transchelation (<5%) was observed after 24 h exposure to a 20-fold excess of TETA at 25 °C, according to radio-HPLC and radio-TLC analyses (Figure S2).

Synthesis and Labeling of EGF Receptor-Targeting Peptide Conjugate. Having demonstrated the capacity for the new pro-chelator to generate a ^{64}Cu(II)-complexing ligand suitable for PET applications, it was incorporated into a peptide-based conjugate to illustrate its utility in multimodal probe construction. For this purpose, the D4 peptide (H_2N-Lys-Ala-Arg-Leu-Leu-Thr-CO_2H) designed *in silico* by Song et al.[55] was employed. The D4 peptide binds to a highly accessible pocket on the surface of the EGF receptor, well separated from the binding site of the endogenous ligand. Although no quantitative binding data has been reported, subsequent conjugation of this peptide to liposomes demonstrated enhanced binding to EGF receptor-expressing tumor cells, both *in vitro* and *in vivo*. In addition to the D4 sequence, the new probe features a TACN-based chelator "clicked" to the side chain of an alkyne-bearing amino acid (β-homopropargylglycine), together with a sulfonated cyanine dye (sulfo-Cy5) for near-infrared (NIR) fluorescence detection (Figure 1).

The peptide conjugate was assembled by solid-phase peptide synthesis (SPPS) methods. The initial strategy attempted was to first couple the sulfo-Cy5 dye to the N-terminus of the peptide and then to click **1** to the β-homopropargylglycine residue to form the product. Although attachment of the dye proceeded smoothly, the click reaction proved troublesome, with no trace of product observed when the reaction was attempted either on the resin-bound peptide or on fully cleaved and deprotected, HPLC-purified peptide. This could be due to the alkyne group of the β-homopropargylglycine residue being insufficiently accessible for **1** to react. Given these difficulties, an alternative synthetic strategy involving the preconjugation of **1** to Fmoc-L-β-homopropargylglycine (Scheme 3) was trialed. While this reaction proceeded slowly under ambient conditions, microwave heating led to efficient conversion to the clicked amino acid product (**4**). Subsequent preparative HPLC provided highly pure **4** in reasonable overall yield (52%), free from any copper contaminants (it should be noted that the two Boc protecting groups in **3** prevent the tacn ring from chelating the Cu(I) catalyst employed in the click reaction). From here, **4** was employed as a typical amino acid building block in the construction of the peptide conjugate by SPPS. Coupling of **4** to the growing peptide proceeded well under standard HCTU coupling conditions, and the conjugate was obtained in high purity (95%), following preparative HPLC (10% yield). The cysteine residue, incorporated to allow future attachment to, for example, nanoparticles, was capped with maleimide for the purposes of this study.

The peptide conjugate was efficiently radiolabeled (>95% radiochemical purity) by incubating with $^{64}Cu^{2+}$ ions for 30 min at 25 °C and pH 5.5 (0.1 M MES). The resulting radioconjugate exhibited strong resistance to demetalation, with only 3% of the initial radioactivity leached from the conjugate upon addition to human serum; a further 3% was lost after 2 h incubation at 37 °C, increasing to 16% after 24 h.

Investigation of EGF Receptor-Binding Properties of Peptide Conjugate. As noted earlier, the D4 peptide was designed as an EGF receptor-targeting agent.[55,57,58] However, to date, no study has definitively confirmed binding of this peptide to the receptor, or measured the apparent dissociation constant (K_d) for the interaction. In light of this, the EGF receptor-binding characteristics of our new peptide conjugate probe were investigated.

Laser fluorescence spectroscopy measurements performed on dilute solutions (0–100 nM) of the peptide conjugate revealed a significant enhancement in the emission from the sulfo-Cy5 dye upon the addition of 100 ng mL^{-1} (0.6 nM) of pure EGF receptor protein (Figure 4). These observations are consistent with the formation of a adduct between the conjugate and the receptor, with the dye experiencing a dramatic change in its microenvironment from a highly solvated

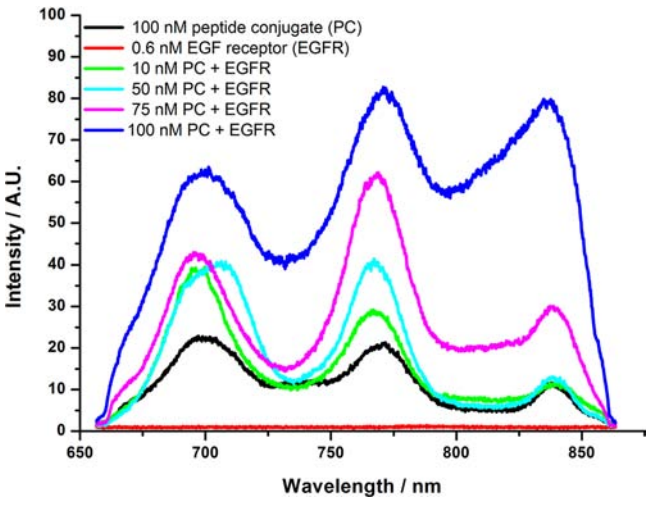

Figure 4. Fluorescence spectra recorded of solutions of the peptide conjugate (PC, 100 nM) (black curve), the EGF receptor (EGFR, 0.6 nM) (red curve), and mixtures of the peptide conjugate with EGF receptor present at a fixed concentration of 0.6 nM.

dx.doi.org/10.1021/bc5001388 | *Bioconjugate Chem.* 2014, 25, 1011–1022

one to a more hydrophobic one upon binding to the receptor surface.

The ability of the peptide conjugate to bind to the EGF receptor was further demonstrated in experiments performed with three human cancer cell lines: the EGF receptor-negative MDA-MB-35S cell line (no detectable EGF receptor), the moderate EGF receptor-expressing FaDu cell line ($(4.5 \pm 2.1) \times 10^6$ receptors cell^{-1}), and highly EGF receptor-expressing A431 cell line ($(4.8 \pm 1.4) \times 10^7$ receptors cell^{-1}). The peptide conjugate–EGF receptor complex could be immunoprecipitated from FaDu and A431 cell lysates using Sepharose beads coated with anti-EGF receptor antibodies. Further, after detachment from the beads with 0.1% SDS, the intact complex could be separated by SDS-PAGE and definitively identified using a combination of radiography (^{64}Cu), fluorescence (sulfo-Cy5), and immunoblotting (Figure 5), indicative of a strong ligand–receptor interaction (neither peptide conjugate-treated MDA-MB-S35 cell lysates nor the peptide conjugate alone produced immunoprecipitates).

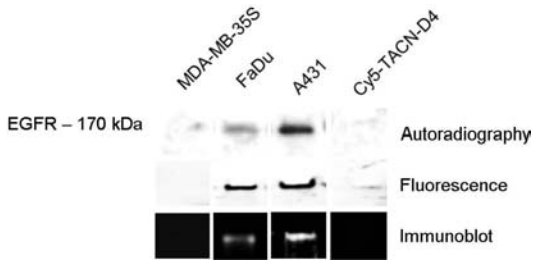

Figure 5. Identification of peptide conjugate–EGF receptor complex, coimmunoprecipitated from FaDu and A431 cell homogenates with anti-EGF receptor antibody-labeled Sepharose beads after incubation of the cells with the conjugate. The top row of panels shows the radioactivity in the SDS-PAGE gel arising from the ^{64}Cu-labeled conjugate (four sections from the same gel). The middle row of panels shows the fluorescence from the sulfo-Cy5 dye of the conjugate (four sections from the same gel). The bottom row of panels shows immunoblots of the gel, using specific antibodies to detect the EGF receptor (four sections from the same immunoblot). The colocalization of the bands confirms formation of a stable peptide conjugate–EGF receptor complex. Since it was not possible to detect both the ^{64}Cu and sulfo-Cy5 labels on the same gel/blot, two typical gels/blots from four independent experiments are shown. Radioactively labeled proteins could be detected only on gels but rarely after blotting. A 10-fold higher amount of radioactivity was found on the cathode compared to the blot membrane and the anode after blotting. It therefore appears that the high electric field employed during the blotting process causes stripping of the ^{64}Cu from the chelator. The complete gels and immunoblot are shown in Figure S5.

Fluorescence microscopic imaging of A431 cells treated with the peptide conjugate and fluorescent antibodies targeting the EGF receptor clearly showed fluorescence arising from the sulfo-Cy5 dye, which overlapped to a high degree (70% colocalization) with the signal from fluorescent antibodies (Figure S3). In contrast, the EGF receptor-negative MDA-MB-35S cells treated in a similar fashion showed minimal fluorescence emanating from either the probe or the anti-EGF receptor antibodies.

Determination of Apparent Dissociation Constant for Peptide Conjugate–EGF Receptor Complex. In order to determine the apparent dissociation constant for the interaction of the peptide conjugate with the EGF receptor, varying amounts of the ^{64}Cu(II)-labeled conjugate were incubated separately with suspensions of cells from the three different cell lines containing the same amount of EGF receptor protein (as determined by ELISA), and the amount of bound and unbound conjugate determined from the amount of radioactivity detected on a glass microfiber filter and in the filtrate after vacuum filtration (sulfo-Cy5 fluorescence could not be quantified with the required accuracy). A similar experiment performed with the addition of a 500-fold excess of nonradioactively labeled peptide conjugate revealed that ca. 20% of the bound radioactivity was associated with nonspecific binding. A Scatchard plot of the data corrected for this effect was linear ($R^2 = 0.88$), indicating formation of a 1:1 conjugate–EGF receptor complex, and fitting of the data to formation of a 1:1 complex yielded an apparent dissociation constant of 12 ± 7 nM based on the FaDu cell binding data, and 4 ± 2 nM based on the A431 cell binding data (means $\pm$ SD of three independent experiments). These values are in the range measured for binding of other ligands to the EGF receptor, e.g., the GE11 peptide (K_d = 22 mM).[54] It is likely that the sulfo-Cy5 dye strengthens the interaction between the conjugate and the EGF receptor through a hydrophobic effect, as proposed recently by Ongarora et al.[57] for a series of phthalocyanine dye peptide conjugates targeting the EGF receptor.

As part of this study, K_d values of 50 ± 9 pM and 5.6 ± 1.7 nM were measured for the binding of EGF to the EGF receptor in FaDu cells, and 40 ± 2 pM and 0.5 ± 0.2 nM for binding to the receptor in A431 cells. These values are comparable to the values of 70 pM and 5 nM reported by Kawamoto et al.[61] and correspond to the binding of EGF to an isolated receptor ("high affinity" site), which induces receptor dimerization, followed by binding to a second receptor ("low affinity" site).[62,63]

Investigation of Impact of Peptide Conjugate Binding on EGF Receptor Activation in A431 Cells. The binding of EGF to the EGF receptor activates the intrinsic protein kinase activity of the receptor, which leads to several phosphorylations within its cytoplasmic domain and initiation of a number of signal transduction cascades.[64,65] In order to deduce the effect of binding of the peptide conjugate on EGF receptor-mediated signaling, a series of immunoblot experiments were carried out to detect the phosphorylation state of specific EGF receptor residues after exposure of A431 cells to the conjugate and/or the native EGF ligand.

As shown in Figure 6, binding of the conjugate was found to induce phosphorylation of Thr669 in a concentration-dependent manner, and to a degree comparable with EGF. Interestingly, however, simultaneous addition of the conjugate and EGF did not amplify the degree of phosphorylation in an additive fashion, as might have been anticipated from the fact that both effectors bind to different sites on the receptor, although this may simply be because saturation was reached. The Thr669 residue is phosphorylated by a p38 mitogen-activated protein kinase (MAPK) and is involved in ligand-induced receptor internalization, leading to a transient down-regulation of the EGF receptor.[66]

The peptide conjugate was also found to induce autophosphorylation of the Tyr992 residue of the EGF receptor in a concentration-dependent manner, but to a much lesser extent (ca. 10%) compared to EGF (Figure 6). Tyr992 phosphorylation is known to trigger the binding and activation of phospholipase C_γ (PLC_γ),[67] which in turn activates phosphokinase C (PKC), leading to signaling via extracellular signal-regulated kinase (ERK) and MAPKs,

dx.doi.org/10.1021/bc5001388 | Bioconjugate Chem. 2014, 25, 1011–1022

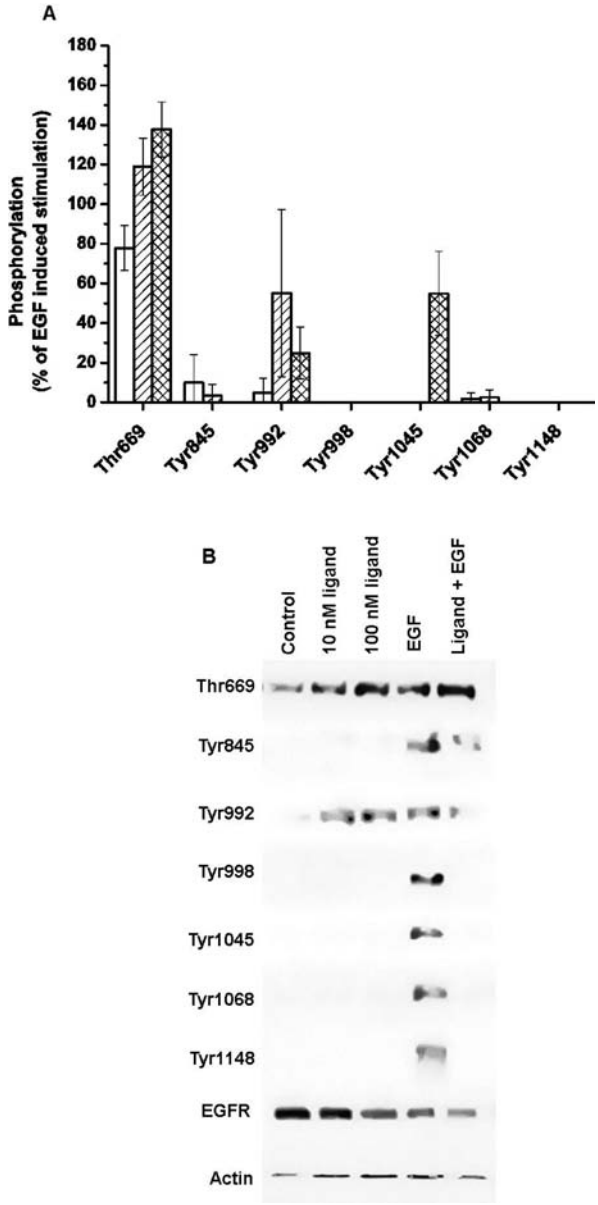

Figure 6. Analysis of EGF receptor phosphorylation induced by binding of the peptide conjugate and EGF, either alone or in combination. (A) Measured degrees of phosphorylation of specific residues induced by exposure to 10 (open colums) or 100 nM (hatched colums) peptide conjugate, or simultaneous treatment with 100 nM conjugate and 16 nM EGF (criss-crossed colums). The values are expressed as a percentage of the phosphorylation level induced by EGF alone, and are normalized relative the phosphorylation levels observed for the EGF receptor after 24 h serum starvation (error bars correspond to the standard deviation in the results obtained from three independent experiments). (B) Representative immunoblots showing the phosphorylation state of specific residues after exposure of the EGF receptor to the peptide conjugate/and or EGF, as detailed in (A).

including the p38 pathway.[68] Autophosphorylation of the other investigated residues (Tyr845, Tyr998, Tyr1045, Tyr1068, and Tyr1148) was found to be minimal in the presence of the peptide conjugate, indicating that the peptide conjugate functions as a biased or partial agonist. Significantly, EGF-stimulated phosphorylation of the latter residues was also found to be greatly reduced or almost completely suppressed upon simultaneous addition of the conjugate with EGF. Given that the D4 peptide binds to a highly solvent-exposed site on EGFR[56] that is distinct from the EGF-binding pocket,[69] a likely explanation for this effect is that binding of the peptide conjugate hinders the EGF-induced receptor dimerization process required for activation of the kinase domains responsible for autophosphorylation of the Tyr845, Tyr998, Tyr1045, Tyr1068, and Tyr1148 residues.[70,71] This indicates that the peptide conjugate also functions as a noncompetitive antagonist. In addition to representing an effective targeting vector, the D4 peptide therefore has scope for development into a new anticancer therapeutic agent that functions by countering the proliferative effects of overexpressed or mutants EGF receptors present on the surface of various cancer cells.

■ CONCLUSION

We have developed a novel "clickable" TACN-based pro-chelator compound and successfully employed it in the construction of a new EGF receptor-targeting probe based on the previously reported D4 peptide.[55] The chelating moiety within the peptide conjugate is capable of complexing $^{64}Cu^{2+}$ ions for radioactivity-based detection, and is resistant to transchelation. Moreover, detailed studies have confirmed that the conjugate forms a very stable complex with the EGF receptor ($K_d \sim 10$ nM) and that the formation of this complex inhibits EGF-induced autophosphorylation of a number of tyrosine residues crucial for EGF receptor-mediated signal transduction. Taken together, these results indicate that both the new pro-chelator and peptide-based probe will be useful for multimodal imaging applications and the construction of EGF receptor-targeted nanomedicine platforms. As part of our ongoing research, we plan to exploit the new peptide conjugate as an advanced building block in the construction of new nanoparticle-based theranostic agents suitable for PET, MRI, and fluorescence imaging of cancerous tumors *in vivo*, in combination with radiotherapy and/or hyperthermia.

■ EXPERIMENTAL SECTION

Materials and Methods. All commercially sourced chemicals were of reagent or analytical grade. Sulfo-Cy5 NHS ester was purchased from Lumiprobe GmbH (Hannover, Germany) and Fmoc-L-β-homopropargylglycine was purchased from Chem-Impex International, Inc. (Wood Dale, IL, USA). All solvents used were of analytical or HPLC grade. Dried solvents were obtained with the MB-SPS 800 purification system from M. Braun. Milli-Q water was used consistently throughout. ^{64}Cu was produced on the "Cyclone 18/9" PET cyclotron of the Helmholtz-Center Dresden-Rossendorf by the $^{64}Ni(p,n) \rightarrow {}^{64}Cu$ nuclear reaction, according to Thieme et al.[10]

Instrumentation. *Microwave syntheses* were performed on CEM Discover SP Series microwave synthesizer. *Nuclear Magnetic Resonance (NMR) spectra* were recorded on an Avance III Nanobay 400 MHz Bruker spectrometer coupled to the BACS 60 automatic sample changer. Data acquisition and processing was managed using MestReNova version 8.0.0–10524 and iNMR version 3.1.4. Abbreviations used to describe ^1H NMR spectra are s (singlet), d (doublet), t (triplet), q (quartet), dd (doublet of doublets), m (multiplet), or br (broad). *High resolution-mass spectrometry (HRMS)* was performed on a Waters LCT TOF LC/MS mass spectrometer coupled to a 2795 Alliance Separations module. All data were acquired and mass-corrected via a dual-spray Leucine Enkephaline reference sample. The mass spectrum was created by

dx.doi.org/10.1021/bc5001388 | Bioconjugate Chem. 2014, 25, 1011–1022

averaging the scans across each peak and subtracting the background of the TIC. Acquisition and analysis was performed using the Masslynx software version 4.1. *Microanalyses (C, H, and N)* were performed on a EuroVector EA-3000 elemental analyzer. *Ultraviolet and visible (UV−vis) spectra* were recorded on a Cary 50 Bio UV−visible absorption spectrophotometer. *Liquid chromatography−mass spectrometry (LCMS)* was performed using an Agilent 6100 Series Single Quad LC/MS, incorporating a photodiode array detector (214/254 nm) coupled directly to an electrospray ionization source. *Analytical high-performance liquid chromatography (HPLC)* was carried out on the Waters 2690 separation module coupled with a Waters 996 photodiode array detector with a Phenomenex Luna C-8 column (100 Å, 5 μm, 150 × 4.6 mm). *Preparative HPLC* was performed on a Waters Prep LC controller with a Waters 486 tunable absorbance detector using a Phenomenex Luna C-8 column (100 Å, 10 μm, 250 × 50.0 mm). *Radio-HPLC* was performed on a Knauer HPLC fitted with a radio-detector using a Phenomenex Aqua C-18 column (125 Å, 5 μm, 250 × 4.6 mm). 99.9% H_2O/0.01% TFA ("Buffer A") and 79.9% H_2O/20% CH_3CN/0.01% TFA ("Buffer B") elution buffers were used for all HPLC. *Radio-TLC* chromatograms were scanned using a radioisotope thin layer analyzer (Rita Star, Raytest). *Time-resolved laser-induced fluorescence spectroscopy (TRLFS)* was performed on a state-of-the-art system incorporating a tunable solid state laser (Newport-Spectra-Physics), a spectrograph (Acton Research; 600 lines mm^{-1} grating, center wavelength 670 nm for measurement of sulfo-Cy5 fluorescence), and an intensified CCD camera system (Roper Scientific) positioned at right angles to the excitation laser. *Fluorescence microscopy* was carried out on an inverse microscope (Axio Observer) equipped with a Colibri LED illumination system, a HBO light source, and a CCD camera (AxioCam), with image acquisition and processing performed with the AxioVision software platform. All calculations and graphical analyses were performed using OriginPro 8.6 (OriginLab Corporation, Northampton, MA, USA).

Syntheses. *Di-tert-butyl 7-((6-(Azidomethyl)pyridin-2-yl)-methyl)-1,4,7-triazacyclononane-1,4-dicarboxylate (**1**).* 2,6-*bis*(Bromomethyl)pyridine[72] (4.09 g, 15.4 mmol) was combined with NaN_3 (1.30 g, 20.1 mmol) in CH_3CN, and stirred at 60 °C for 18 h. Once the solution had cooled to room temperature (RT), the unreacted NaN_3 was filtered off. Di-*tert*-butyl-1,4,7-triazacyclononane-1,4-dicarboxylate[73] (1.42 g, 4.31 mmol) and K_2CO_3 (1.19 g, 8.62 mmol) were added to the filtrate and the mixture was heated to reflux overnight. After cooling to RT, the reaction mixture was filtered to remove any insoluble salts. The collected filtrate was concentrated under reduced pressure, and the resulting crude product purified by silica flash chromatography (30% EtOAc in petroleum spirits) to give a clear brown waxy solid (411 mg, 62%). ^{1}H NMR (400 MHz; $CDCl_3$): δ 7.79 (t, J = 7.2 Hz, 1H), 7.53 (d, J = 7.2 Hz, 1H), 7.35 (d, J = 7.4 Hz, 1H), 4.67 (s, 2H), 4.42 (s, 2H), 4.07−3.71 (m, 4H), 3.55−3.32 (m, 8H), 1.59−1.40 (m, 18H). ^{13}C NMR (101 MHz, $CDCl_3$) δ 160.82, 155.91, 154.64, 137.39, 122.62, 120.30, 79.84, 62.30, 55.72, 54.54, 54.24, 53.53, 53.41, 52.14, 51.25, 50.79, 50.62, 50.06, 49.43, 48.84, 28.74, 28.67. HRMS ($C_{23}H_{37}N_7O_4$): Calc'd 476.2985 $[M + H]^+$. Found 476.2982. Analytical HPLC: 96% purity (254 nm).

*Di-tert-butyl 7-((6-((4-(Hydroxymethyl)-1H-1,2,3-triazol-1-yl)methyl)pyridin-2-yl)methyl)-1,4,7-triazacyclonane-1,4-dicarboxylate (**2**).* Compound **1** (138 mg, 0.290 mmol) was dissolved in MeOH (20 mL), followed by the sequential addition of propargyl alcohol (17 μL, 0.29 mmol), *tris*(hydroxypropyltriazolylmethyl)amine (THPTA) (25 mg, 0.0058 mmol), $CuSO_4$ (5 mg, 0.003 mmol), and sodium ascorbate (57 mg, 0.29 mmol). The reaction mixture was stirred for 1 h at RT and then concentrated under reduced pressure. The resulting oily residue was dissolved in CH_2Cl_2 (20 mL) and washed with H_2O (3 × 20 mL). The organic layer was dried over $MgSO_4$, filtered, and concentrated under reduced pressure to yield an orange−brown oil (142 mg, 92%). ^{1}H NMR (400 MHz; $CDCl_3$): δ 7.73−7.69 (m, 1H), 7.64−7.53 (m, 1H), 7.46−7.41 (m, 1H), 7.03−7.01 (m, 1H), 5.57 (m, 2H), 4.77 (s, 2H), 3.83−3.08 (m, 2H), 3.50−3.39 (br, 4H), 3.26−3.16 (m, 4H), 2.72−2.64 (m, 4H), 1.46, 1.45, 1.40, 1.38 (all s, 18H total). ^{13}C NMR (101 MHz, $CDCl_3$) δ 160.75, 155.81, 155.61, 153.44, 137.65, 122.99, 122.42, 120.68, 79.70, 62.10, 56.65, 55.68, 54.32, 53.54, 53.39, 53.19, 50.65, 50.37, 49.99, 49.51, 49.16, 28.69, 28.63. LCMS: m/z (ESI, 20 V) = 532.4 $[M + H]^+$. Analytical HPLC: 98% purity (254 nm).

*(1-((6-((1,4,7-Triazacyclononan-1-yl)methyl)pyridin-2-yl)-methyl)-1H-1,2,3-triazol-4-yl)methanol, TFA Salt (**3**).* Compound **2** (142 mg, 0.267 mmol) was dissolved in a mixture of trifluoroacetic acid (5 mL) and CH_2Cl_2 (5 mL) and left to stir at RT overnight. The reaction mixture was then concentrated under reduced pressure to yield a dark-brown oil (320 mg, quantitative). ^{1}H NMR (400 MHz; MeOD): δ 8.02 (s, 1H), 7.86 (t, J = 7.7 Hz, 1H), 7.47 (d, J = 7.0 Hz, 1H), 7.34 (d, J = 7.9 Hz, 1H), 5.77 (s, 2H), 4.67 (s, 2H), 4.09 (s, 2H), 3.80 (s, 4H), 3.36 (t, J = 5.6 Hz, 4H), 3.05 (t, J = 5.7 Hz, 4H). ^{13}C NMR (101 MHz, MeOD): δ 159.96, 155.30, 149.72, 140.24, 124.73, 124.60, 123.4, 56.33, 50.90, 46.90, 46.22. HRMS ($C_{16}H_{25}N_7O$): Calc'd 332.2199 $[M + H]^+$. Found 332.2187. Analytical HPLC: 96% purity (254 nm).

*(1-((6-((1,4,7-Triazacyclononan-1-yl)methyl)pyridin-2-yl)-methyl)-1H-1,2,3-triazol-4-yl)methanolcopper(II) Diperchlorate Monohydrate (**C1**).* Compound **3** (25 mg, 0.028 mmol) and $CuCl_2$ (8 mg, 0.06 mmol) were dissolved in 5 mL H_2O, and the pH was adjusted to ca. 5 with 1 M NaOH, resulting in a deep-purple colored solution. Addition of excess $NaClO_4$ (0.5 g, 4 mmol) followed by slow evaporation over 2 days yielded a dark-purple precipitate (9 mg, 55%). Elemental analysis: ($C_{16}H_{25}Cl_2CuN_7O_9$, MW = 593.86 g mol^{-1}): Calc'd C, 32.36; H, 4.24; N, 16.51. Found C, 33.02; H, 4.46; N, 16.43. UV−vis (H_2O): λ_{max} (nm) [ε_{max}] (M^{-1} cm^{-1}): 580 [102]. X-ray crystallographic quality single-crystals of the complex (as a monohydrate) were grown by slowly diffusing Et_2O into a methanolic solution of **C1**.

*4-(1-((6-((4,7-Bis(tert-butoxycarbonyl)-1,4,7-triazacyclononan-1-yl)methyl)pyridin-2-yl)methyl)-1H-1,2,3-triazol-4-yl)-3-(((((9,9a-dihydro-4aH-fluoren-9-yl)methoxy)carbonyl)-amino)butanoic Acid (**4**).* Compound **1** (150 mg, 0.315 mmol) and Fmoc-L-β-homopropargylglycine (111 mg, 0.315 mmol) were dissolved in MeOH (5 mL), prior to the addition of THPTA (27 mg, 0.063 mmol), $CuSO_4$ (10 mg, 0.063 mmol), and sodium ascorbate (125 mg, 0.630 mmol). The reaction mixture was heated at 100 °C for 10 min in a microwave reactor. The obtained residue was purified by preparative HPLC (60 min gradient from 100% A to 60% B; flow rate 10 mL min^{-1}) to yield an off-white powder after lyophilization (131 mg, 52%). ^{1}H NMR (400 MHz; MeOD): δ 7.81 (s, 1H), 7.80 (m, 2H), 7.61 (b, 1H), 7.57 (d, J = 7.5 Hz, 1H), 7.51 (d, J = 7.3 Hz, 2H), 7.40 (q, J = 7.2 Hz, 2H), 7.31 (q, J = 6.9 Hz, 2H), 7.19 (d, J = 7.7 Hz, 1H), 5.61 (m, 2H), 4.55 (m, 2H), 4.27 (b, 1H), 4.03 (br, 1H), 4.00 (br, 1H), 3.73 (br,

dx.doi.org/10.1021/bc5001388 | *Bioconjugate Chem.* 2014, 25, 1011−1022

4H), 3.45 (br, 4H), 3.35, (br, 4H), 2.89 (m, 2H), 2.60 (m, 2H), 1.50 (s, 18H). ^{13}C NMR (101 MHz, MeOD): δ 174.24, 156.3, 155.80, 146.16, 145.17, 142.39, 140.03, 128.43, 128.07, 126.4, 126.28, 124.92, 123.91, 121.01, 82.89, 67.59, 60.06, 55.00, 52.77, 44.70, 48.74, 49.47, 47.82, 40.09, 31.81, 28.24. HRMS ($C_{44}H_{56}N_8O_8$): Calc'd 825.4299 $[M + H]^+$. Found 825.4324. Analytical HPLC: 98% purity (254 nm).

Peptide Conjugate. The peptide sequence Cys-β-Ala-β-Ala-Gly-Leu-Ala-Arg-Leu-Leu-Thr was constructed on a 2-chlorotrityl polymer resin preloaded with 0.67 mequiv g^{-1} of L-Thr(^{t}Bu) (149 mg, 0.100 mmol) using a PS3 Automated Peptide Synthesizer (Protein Technologies Inc.). Fmoc-protected L-amino acids (0.300 mmol) and standard automated coupling and deprotection protocols were employed, with 2-(6-chloro-1*H*-benzotriazole-1-yl)-1,1,3,3-tetramethylaminium hexafluorophosphate (HCTU) as the activating agent (124 mg, 0.300 mmol) and 20% piperidine in DMF used for Fmoc deprotections. After washing with DMF, MeOH, and Et_2O (3 × 3 mL each), a portion of the dried resin (ca. 0.01 mmol loading of peptide) was transferred to 5 mL syringe (fitted with a frit), swelled in DMF (1 mL) for 30 min, and then gently mixed with a freshly prepared solution of **4** (50 mg, 0.061 mmol), HCTU (26 mg, 0.063 mmol), and DIPEA (40 μL, 0.23 mmol) in DMF (2 mL) for 2 h. The resin was next washed with DMF (3 × 3 mL) and the terminal Fmoc group removed by treating with 20% piperidine in DMF (2 × 4 mL for 5 min). After washing with DMF (2 × 4 mL), a solution of sulfo-Cy5-NHS (18 mg, 0.020 mmol) and DIPEA (17 μL, 0.10 mmol) in DMF (2 mL) was added, and the mixture gently mixed for 2 h. The resin was then washed with DMF, MeOH, and Et_2O (3 × 3 mL each), before cleavage of the final peptide was achieved by treatment with a mixture of 2.5% triisopropylsilane (TIPS), 2.5% 3,6-dioxa-1,8-octanedithiol (DODT), 95% TFA (1 mL) for 2 h. The spent resin was removed by filtration, the filtrate was concentrated using a gentle stream of nitrogen, and Et_2O (10 mL) was added to initiate precipitation of the peptide. After cooling at 4 °C for 2 h, the precipitate was pelleted by centrifugation, washed with Et_2O (3 × 5 mL), and dried under reduced pressure, before being purified to by preparative HPLC (60 min gradient from 100% A to 80% B; flow rate 10 mL min^{-1}) to yield a deep-blue powder after lyophilization (19 mg, 10%). HRMS ($C_{91}H_{138}N_{22}O_{19}S_3$): Calc'd 647.3302 $[M+3H]^{3+}$. Found 647.6647. Analytical HPLC: 95% purity (254 nm). The cysteine residue within the peptide was capped by stirring a solution of the peptide (10 mg, 0.0050 mmol) and maleimide (2 mg, 0.02 mmol) in 0.1 M 2-(*N*-morpholino)ethanesulfonic acid (MES) buffer (pH 6.0) (2 mL) for 4 h. The product was purified by preparative HPLC (60 min gradient from 100% A to 80% B; flow rate 10 mL min^{-1}) and lyophilized to yield a deep-blue powder (8 mg, 80%). HRMS ($C_{95}H_{141}N_{23}O_{21}S_3$): Calc'd 679.6690 $[M+3H]^{3+}$. Found 679.8353. Analytical HPLC: 96% purity (254 nm).

X-ray Crystallography. Intensity data for blue crystals of **C1** (0.25 × 0.20 × 0.05 mm^3) were measured at 123 K on a Bruker Apex II CCD fitted with graphite monochromated Mo Kα radiation (0.71073 Å). The data were collected to a maximum 2θ value of 55° and processed using the Bruker Apex II software package. Crystal parameters and details of the data collection are summarized in Table S1 in the Supporting Information. The structure was solved using standard Fourier routines in the SHELX-97.[74] The hydrogen on the oxygen atom (O1 and O2) of the triazole-linked alcohol pendant and the nitrogen atoms on the TACN ring were located on the Fourier difference map and refined with restrained O−H and N−H distances. The isotropic thermal parameters for N−H and O−H hydrogen atoms were fixed at 1.2 times that of the respective nitrogen or oxygen atom. All the remaining hydrogen atoms were placed in idealized positions. The hydrogen atoms associated with the water molecule of crystallization could not be located on the Fourier difference map. The CH_2OH connected to the triazole ring on cationic unit Cu2, perchlorate counteranions, and one of the water molecules were disordered and refined anisotropically.

^{64}Cu(II) Radiolabeling Kinetics and Chelator Challenge Experiment. Compound **3** (10 μg, 0.020 μmol) was combined with 5 MBq of $[^{64}Cu]CuCl_2$ in 0.1 MES buffer (pH 5.5) to make up a final volume of 200 μL. This mixture was incubated with shaking at 25 °C and the extent of $^{64}Cu^{2+}$ ion complexation monitored at various time intervals (1, 3, 5, 30, 60, 120, and 240 min) by radio-TLC (neutral alumina plates run with a 2 M NH_4OAc/MeOH (1:1 v/v) eluent system) and radio-HPLC (40 min gradient from 100% A to 65% B; flow rate 1 mL min^{-1}). For the challenge experiment, **3** (10 μg, 0.020 μmol) was combined with 5 MBq of $[^{64}Cu]CuCl_2$ in 0.1 M MES buffer (pH 5.5) to make up a final volume of 200 μL. After incubating at 37 °C for 45 min, 20 mol equiv of 1,4,8,11-tetraazacyclotetradecane-1,4,8,11-tetraacetic acid (TETA) (173 μg, 0.400 μmol) were added. The mixture was incubated at 25 °C and the amount of intact ^{64}Cu(II) complex of **3** determined at various time intervals (5, 10, 30, 60, 120, 240 min, and 24 h) by radio-TLC (neutral RP18 silica plates run with a 2 M NH_4OAc/MeOH (1:1 v/v) eluent system). Radio-HPLC was also used to assess the stability of the ^{64}Cu(II)-**3** complex at separate time intervals (1, 2, 3, 24 h).

^{64}Cu(II) Radiolabeling of Peptide Conjugate and Serum Stability Measurements. $[^{64}Cu]CuCl_2$ (10 MBq) was added to a stock solution of the peptide conjugate (10 mg mL^{-1}) in 0.1 M MES (pH 5.5) to achieve a conjugate concentration of 1 mg mL^{-1}. The pH was checked and adjusted to 5.5 if necessary. The reaction mixture was shaken at RT for 30−90 min and the radiopurity of the labeled conjugate assessed by radio-TLC (neutral alumina plates run with a 2 M NH_4OAc/MeOH (1:1 v/v) eluent system) and radio-HPLC (40 min gradient from 100% A to 65% B; flow rate 1 mL min^{-1}).

Serum stability was assessed by incubating aliquots of the radiolabeled peptide conjugate solution with human serum (Sigma-Aldrich) in a 1:2 (v/v) ratio at 37 °C. The amount of intact radiolabeled peptide conjugate was quantified after 0, 2, and 24 h by radio-TLC (neutral alumina plates run with a 2 M NH_4OAc/MeOH (1:1 v/v) eluent system).

Analysis of Interaction of Peptide Conjugate with EGF Receptor via TRLFS. The fluorescence spectra of solutions containing a fixed concentration of human EGF receptor protein (isolated form A431 cells, Enzo Life Sciences GmbH, Lörrach, Germany) (0.6 nM) and varying concentrations of peptide conjugate (0, 10, 50, 75, and 100 nM) in phosphate-buffered saline (PBS) (preincubated for 30 min at 4 °C) were recorded using an excitation wavelength of 600 nm, a gate time of 1 μs, and a delay time of 30 ns.

Cell Culture and Determination of EGF Receptor Density. The MDA-MB-435S and A431 cell lines were purchased from CLS Cell Lines Service GmbH (Eppelheim, Germany) and the FaDu (HTB-43) cell line from LGC Standards GmbH (Wesel, Germany). All culture media and supplements were purchased from Biochrom AG, Berlin,

Germany). The cells were maintained in either RPMI medium (MDA-MB-435S and FaDu) or Dulbecco's modified Eagle's medium (DMEM) (A431) supplemented with 10% standardized fetal bovine serum (FBS), at 37 °C in a humidified atmosphere enriched with 5% CO_2. Determination of the EGF receptor density for each cell line was performed in 96-well plates (3000 cells well^{-1}, Cellstar, Greiner Bio-One GmbH, Frickenhausen, Germany) by treating the cells with fluorescein-labeled EGF (dosed in ca. 5-fold excess), washing away unbound labeled EGF with phosphate buffered saline (PBS), and then quantifying the degree of binding using a fluorescence plate-reader (VarioskanFlash, Thermo Fisher Scientific, Bonn, Germany). The labeled EGF was prepared according a protocol established by Azevedo and Johnson,[75] except that excess fluorescein excess was removed via ultrafiltration (Vivaspin 500, MWCO 3000 Da, Sartorius Stedim Biotech GmbH). Binding of the labeled EGF to EGF receptors was confirmed by SDS-PAGE and subsequent immunoblotting (data not shown).

The EGF receptor content of the cells was also determined using an enzyme-linked immunosorbent assay (ELISA). For this, cell samples were prepared by detaching the cells from the culture flasks with 0.05% Trypsin/0.02% EDTA solution, washing three times with PBS and finally mechanical disruption using a pestle. The cells were resuspended in diluted ELISA coating buffer (5×) (BioLegend GmbH, Fell, Germany) and incubated overnight at 4 °C in transparent 96-well plates (Microlon 600, Greiner Bio-One GmbH, Frickenhausen, Germany). After intensively washing and blocking (5% milk powder in tris(hydroxymethyl)aminomethane (Tris)-buffered saline (TBS), immunoreactions were performed using, first, EGF receptor antibody (C-20, 1:30 dilution, Santa Cruz Biotechnology Inc., Heidelberg, Germany) and, second, an anti-goat-horseradish peroxidase (HRP)-conjugated antibody (1:1000 dilution, Santa Cruz Biotechnology Inc.). HRP reaction was initiated with 3,3′,5,5′-tetramentylbenzidine (1-StepUltra TMB-ELISA, Thermo Fisher Scientific, Bonn, Germany). After stopping the reaction with sulfuric acid, the absorption of the resulting yellow solution was read at 450 nm using a plate reader (VarioskanFlash, Thermo Fisher Scientific) to determine the EGF receptor concentration. A calibration curve was constructed using purified EGF receptor (Enzo Life Sciences GmbH).

Analysis of Interaction of Peptide Conjugate with EGF Receptor via Immunoprecipitation, SDS-PAGE, and Western Blotting. Cell lysates were prepared by detaching cells from culture flasks with 0.05% Trypsin/0.02% EDTA solution and washing three times with PBS. The resulting cell pellets were resuspended in PBS supplemented with 0.05% deoxycholate, 0.05% dodecyl-β-D-maltoside, and nuclease, mechanically disrupted with a pestle and solubilized on ice for 1 h. The cell lysates were then cleared by centrifugation at 15 000 rpm for 20 min at 4 °C, and the protein content measured using the commercially available DC Protein Assay Kit (Bio-Rad Laboratories GmbH, Munich, Germany) with bovine serum albumin (BSA) standards. The supernatants were incubated with the peptide conjugate (100 μg mL^{-1}) at 37 °C for 30 min. Subsequently, Sepharose beads conjugated with EGF receptor (D38B1) XP monoclonal rabbit antibodies (Cell Signaling Technology (CST), Frankfurt/M, Germany) were added and the mixtures incubated with gentle rocking for 4 h at 4 °C. After brief centrifugation, the pellets were washed five times with ice-cold PBS. The resulting EGF receptor−antibody complexes were resuspended by vortexing in native sample buffer (Bio-Rad Laboratories GmbH), including 0.1% sodium dodecyl sulfate (SDS), and then subjected to SDS polyacrylamide gel electrophoresis (SDS PAGE) according to Laemmli.[76] Autoradiography of the gel was performed using a phosphoimager (FujiFilm BAS-3000, Raytest Isotopenmessgeräte GmbH, Straubenhardt, Germany). Fluorescent bands were detected by scanning the gel with a high sensitivity multiplex fluorescence gel imaging system (Molecular Imager PharosFX Plus, Bio-Rad Laboratories) using the appropriate laser wavelength for sulfo-Cy5. Following this, the gel was semi-dry-blotted onto nitrocellulose (Protran, Whatman/Schleicher & Schuell) at 4 °C overnight using 25 mM Tris, 20% methanol (pH 10.4) as the anode buffer, and 25 mM Tris, 20% methanol, 40 mM 6-aminocaproic acid (pH not adjusted) as the cathode buffer. After membrane blocking, EGF receptor was detected by immunoreaction with EGF receptor (D38B1) XP monoclonal rabbit antibodies (CST) and anti-rabbit HRP-conjugated secondary antibody. Enhanced chemoluminescence reaction (ECL) was run with 20X LumiGLO Reagent (CST) according to the manufacturer's instructions and detected using a Stella 2000 imaging system (Raytest Isotopenmessgeräte GmbH) equipped with a cooled, full-frame CCD camera.

Fluorescence Microscopic Analysis of Interaction of Peptide Conjugate with EGF Receptor-Expressing Cells. A431 cells (or MDA-MB-35S cells as a control) were seeded in 8-well μ-slides 8 well (Ibidi GmbH, Martinsried, Germany) with 4×10^4 cells well^{-1}. After 24 h, the cells were washed three times with PBS and incubated with a final concentration of 100 μg mL^{-1} of the peptide conjugate in PBS at 37 °C in a humidified atmosphere enriched with 5% CO_2 for 30 min. Afterward, the slides were washed with PBS again and the cells fixed on the slides by incubation with fixation buffer (BioLegend GmbH) in the dark for 20 min. After rinsing three times with PBS, samples were blocked by treatment with 5% normal rabbit serum (Jackson ImmunoResearch Ltd., Suffolk, England), 1% BSA, 0.2% Triton X-100 in PBS for 1 h at RT. EGF receptor (D38B1) XP monoclonal rabbit antibodies (Cell Signaling Technology (CST), diluted (1:200) with cell staining buffer (BioLegend GmbH), were then added to the cells for overnight incubation at 4 °C in the dark. Slides were rinsed three times with cell staining buffer, and then incubated with DyLight 488 donkey anti-rabbit IgG secondary antibody (BioLegend GmbH, dilution 1.200) for 1 h. After rinsing three times with cell staining buffer, DNA was counterstained with 5 mg mL^{-1} of 4′,6-diamidino-2-phenylindole (DAPI, BioLegend GmbH) in water. Image sequences of the cells were captured in multichannel fluorescence mode (with λ_{ex} = 470, 590, and 340 nm, and λ_{em} = 525, 645, and 370 nm for DyLight 488, sulfo-Cy5 and DAPI, respectively) from different focus planes (z-stacks). The obtained images were processed by reassignment of the out-of-focus blurred light to its origin (deconvolution) and separation of overlapping fluorescence signals (correction of spectral bleed-through by spectral unmixing). Subsequently, a statistical analysis of the correlation of the fluorescence from the peptide conjugate (sulfo-Cy5) and the EGF receptor (DyLight 488) was performed using a dual-channel image overlay. An automatic threshold was set according to Costes and co-workers,[77] and the extent of colocalization was calculated as per Manders and co-workers.[78]

Determination of Apparent Dissociation Constant (K_d) for Interaction of Peptide Conjugate with EGF Receptor. Cell samples (MDA-MB-35S, FaDu, and A431) were prepared by detaching cells from culture flasks with 0.05%

Trypsin/0.02% EDTA solution, washing three times with PBS, and then mechanically disrupting using a pestle. All investigated cell samples (except those of MDA-MB-35S) were adjusted to 5 μg mL^{-1} EGF receptor protein (determined by ELISA as described above). The cells were incubated with varying concentrations of the ^{64}Cu(II)-labeled peptide conjugate at 4 °C for 30 min. Unbound conjugate (soluble fraction) was separated from bound conjugate by vacuum filtration through glass microfiber filters (GF/C, Whatman, GE Healthcare Europe GmbH, Freiburg, Germany). After washing the filter three times with ice-cold PBS, the radioactivities of the filtrates (unbound conjugate) and filters (bound conjugate) were measured using an automatic gamma-counter (Wizard, PerkinElmer Inc., Waltham, MA, USA). Concentrations of conjugate were calculated using a calibration curve, with nonspecific filter binding (retention of radioactivity on the filter material) and nonspecific conjugate binding (binding of labeled conjugate in the presence of a 500-fold excess of unlabeled conjugate) corrected for. The apparent dissociation constant was determined from the measured data by Scatchard analysis.[79]

Phosphorylation Assays. MDA-MB-35S and A431 cells were grown to 60−70% confluence in 6-well plates (Cellstar, Greiner Bio-One GmbH) and then serum starved for 24 h (to avoid stimulation by endogenous EGF). After washing with PBS, the cells were incubated with either peptide conjugate (10 or 100 nM), EGF (16 nM), or both the conjugate (100 nM) and EGF (16 nM) simultaneously, in the appropriate culture medium without FBS for 30 min. The supernatant was carefully removed and the cells then lysed using RIPA lysis and extraction buffer (Thermo Fisher Scientific). Cellular debris was resuspended with the aid of a bent pipet tip. Protein concentrations were determined as described above and each sample adjusted to the same protein content. SDS-PAGE, Western blotting, and immunoreactions were performed as described above, but this time using a series of antibodies that bind EGFR only when it is phosphorylated at a specific residue (Thr669, Tyr845, Tyr992, Tyr998, Tyr1045, Tyr 1068, or Tyr1148) (CST). Each blot was stripped according to a protocol published by Abcam (Cambridge, UK), allowing for reuse a second time. Protein bands were analyzed using ImageJ (http://rsbweb.nih.gov/ij/index.html).

■ ASSOCIATED CONTENT

Supporting Information

Radio-HPLC and radio-TLC data showing formation and stability of the ^{64}Cu(II) complex of **3**; fluorescent microscopic images of A431 and MDA-MB-35S cells treated with the peptide conjugate; crystallographic data for **C1·H$_2$O**; SDS-PAGE gels and immunoblot used to identify the peptide conjugate−EGF receptor complex. This material is available free of charge via the Internet at http://pubs.acs.org.

■ AUTHOR INFORMATION

Corresponding Authors

*Tel: +49 3512602934; Fax: +49 3512603232. E-mail: k.viehweger@hzdr.de.

*Tel: +49 3512603091; Fax: +49 3512603232. E-mail: h.stephan@hzdr.de.

*Tel: +61 (0)3 99054526; Fax: +61 (0)3 99054597. E-mail: leone.spiccia@monash.edu.

*Tel: +61 (0)3 99039706; Fax: +61 (0)3 99039582. E-mail: bim.graham@monash.edu. Web: bimgrahamgroup.com.

Author Contributions

Katrin Viehweger and Lisa Barbaro contributed equally to the work.

Notes

The authors declare no competing financial interest.

■ ACKNOWLEDGMENTS

We thank M. Matterna for maintenance and preparation of cell cultures and synthesis of fluorescein-labeled EGF. Financial support by Helmholtz Virtual Institute NanoTracking (Agreement Number VH-VI-421), the Helmholtz-Portfolio Topic "Technologie und Medizin − Multimodale Bildgebung zur Aufklärung des In-vivo-Verhaltens von polymeren Biomaterialien"), and by the Australian Research Council through a Discovery Grant (DP130100816), a Discovery Outstanding Researcher Award (to L.S.), and a Future Fellowship (to B.G.) is gratefully acknowledged, as is the award of a 2010 Senior Research Award by the Alexander von Humboldt Foundation to L.S.

■ REFERENCES

(1) Louie, A. Y. (2010) Multimodality imaging probes: design and challenges. *Chem. Rev. 110*, 3146−3195.

(2) Jennings, L. E., and Long, N. J. (2009) 'Two is better than one'-probes for dual-modality molecular imaging. *Chem. Commun. 24*, 3511−3524.

(3) Connett, J. M., Anderson, C. J., Guo, L. W., Schwarz, S. W., Zinn, K. R., Rogers, B. E., Siegel, B. A., Philpott, G. W., and Welch, M. J. (1996) Radioimmunotherapy with a ^{64}Cu-labeled monoclonal antibody: a comparison with ^{67}Cu. *Proc. Natl. Acad. Sci. U.S.A. 93*, 6814−6818.

(4) Blower, P. J., Lewis, J. S., and Zweit, J. (1996) Copper radionuclides and radiopharmaceuticals in nuclear medicine. *Nucl. Med. Biol. 23*, 957−980.

(5) Smith, S. V. (2004) Molecular imaging with copper-64. *J. Inorg. Biochem. 98*, 1874−1901.

(6) Wadas, T. J., Wong, E. H., Weisman, G. R., and Anderson, C. J. (2007) Copper chelation chemistry and its role in copper radiopharmaceuticals. *Curr. Pharm. Des. 13*, 3−16.

(7) Wadas, T. J., Wong, E. H., Weisman, G. R., and Anderson, C. J. (2010) Coordinating radiometals of copper, gallium, indium, yttrium, and zirconium for PET and SPECT imaging of disease. *Chem. Rev. 110*, 2858−2902.

(8) Shokeen, M., and Anderson, C. J. (2009) Molecular imaging of cancer with copper-64 radiopharmaceuticals and positron emission tomography (PET). *Acc. Chem. Res. 42*, 832−841.

(9) Donnelly, P. S. (2011) The role of coordination chemistry in the development of copper and rhenium radiopharmaceuticals. *Dalton Trans. 40*, 999−1010.

(10) Thieme, S., Walther, M., Pietzsch, H.-J., Henniger, J., Preusche, S., Maeding, P., and Steinbach, J. (2012) Module-assisted preparation of ^{64}Cu with high specific activity. *Appl. Radiat. Isot. 70*, 602−608.

(11) Guo, Y., Parry, J. J., Laforest, R., Rogers, B. E., and Anderson, C. J. (2013) The Role of p53 in combination radioimmunotherapy with ^{64}Cu-DOTA-cetuximab and cisplatin in a mouse model of colorectal cancer. *J. Nucl. Med. 54*, 1−9.

(12) Delgado, R., Felix, V., Lima, L. M. P., and Price, D. W. (2007) Metal complexes of cyclen and cyclam derivatives useful for medical applications: a discussion based on thermodynamic stability constants and structural data. *Dalton Trans. 26*, 2734−2745.

(13) Zeglis, B. M., and Lewis, J. S. (2011) A practical guide to the construction of radiometallated bioconjugates for positron emission tomography. *Dalton Trans. 40*, 6168−6195.

(14) Bartholomä, M. D. (2012) Recent developments in the design of bifunctional chelators for metal-based radiopharmaceuticals used in Positron Emission Tomography. *Inorg. Chim. Acta 389*, 36−51.

(15) Cutler, C. S., Hemmkens, H. M., Sisay, N., Huclier-Markai, S., and Jurisson, S. S. (2013) Radiometals for combined imaging and therapy. *Chem. Rev. 113*, 858−883.
(16) Price, E. W., and Orvig, C. (2014) Matching chelators to radiometals for radiopharmaceuticals. *Chem. Soc. Rev. 43*, 260−290.
(17) Juran, S., Walther, M., Stephan, H., Bergmann, R., Steinbach, J., Kraus, W., Emmerling, F., and Comba, P. (2009) Hexadentate bispidine derivatives as versatile bifunctional chelate agents for copper(II) radioisotopes. *Bioconjugate Chem. 20*, 347−359.
(18) Comba, P., Hunoldt, S., Morgen, M., Pietzsch, J., Stephan, H., and Wadepohl, H. (2013) The optimization of pentadentate bispidines as bifunctional chelators for ^{64}Cu positron emission tomography (PET). *Inorg. Chem. 52*, 8131−8143.
(19) Gasser, G., Tijoe, L., Graham, B., Belousoff, M. J., Juran, S., Walther, M., Künstler, J. U., Bergmann, R., Stephan, H., and Spiccia, L. (2008) Synthesis, copper(II) complexation, ^{64}Cu-labeling and bioconjugation of a new bis(2-pyridylmethyl) derivative of 1,4,7-triazacyclononane. *Bioconjugate Chem. 19*, 719−730.
(20) Barreto, J. A., Matterna, M., Graham, B., Stephan, H., and Spiccia, L. (2011) Synthesis, colloidal stability and ^{64}Cu labelling of iron oxide nanoparticles bearing different macrocyclic ligands. *New J. Chem. 35*, 2705−2712.
(21) Bergmann, R., Ruffani, A., Graham, B., Spiccia, L., Steinbach, J., Pietzsch, J., and Stephan, H. (2013) Synthesis and radiopharmacological evaluation of ^{64}Cu-labeled bombesin analogs featuring a bis(2-pyridylmethyl)-1,4,7-triazacyclononane chelator. *Eur. J. Med. Chem. 70*, 434−446.
(22) Pombo-García, K., Zarschler, K., Barreto, J. A., Hesse, J., Spiccia, L., Graham, B., and Stephan, H. (2013) Design, synthesis, characterisation and in vitro studies of hydrophilic, colloidally-stable, ^{64}Cu(II)-labelled, ultra-small iron oxide nanoparticles in a range of human cell lines. *RSC Adv. 3*, 22443−22454.
(23) Mindt, T. L., Struthers, H., García-Garayoa, E., Desbouis, D., and Schibli, R. (2007) Strategies for the development of novel tumor targeting technetium and rhenium radiopharmaceuticals. *Chimia 61*, 725−731.
(24) Struthers, H., Mindt, T. L., and Schibli, R. (2010) Metal chelating systems synthesized using the copper(I) catalyzed azide-alkyne cycloaddition. *Dalton Trans. 39*, 675−696.
(25) Muller, C., Mindt, T. L., de Jong, M., and Schibli, R. (2009) Evaluation of a novel radiofolate in tumour-bearing mice: promising prospects for folate-based radionuclide therapy. *Eur. J. Nucl. Med. Mol. Imaging 36*, 938−946.
(26) Dijkgraaf, I., Rijnders, A. Y., Soede, A., Dechesne, A. C., van Esse, G. W., Brouwer, A. J., Corstens, F. H. M., Boerman, O. C., Rijkers, D. T. S., and Liskamp, R. M. J. (2007) Synthesis of DOTA-conjugated multivalent cyclic-RGD peptide dendrimers via 1,3-dipolar cycloaddition and their biological evaluation: implications for tumor targeting and tumor imaging purposes. *Org. Biomol. Chem. 5*, 935−944.
(27) Knoer, S., Modlinger, A., Poethko, T., Schottelius, M., Wester, H.-J., and Kessler, H. (2007) Synthesis of novel 1,4,7,10-tetraazacyclodecane-1,4,7,10-tetraacetic acid (DOTA) derivatives for chemoselective attachment to unprotected polyfunctionalized compounds. *Chem.—Eur. J. 13*, 6082−6090.
(28) Viguier, R. F. H., and Hulme, A. N. (2006) A sensitized europium complex generated by micromolar concentrations of copper(I): Toward the detection of copper(I) in biology. *J. Am. Chem. Soc. 128*, 11370−11371.
(29) Mindt, T. L., Struthers, H., Brans, L., Anguelov, T., Schweinsberg, C., Maes, V., Tourwé, D., and Schibli, R. (2006) ″Click to chelate″: Synthesis and installation of metal chelates into biomolecules in a single step. *J. Am. Chem. Soc. 128*, 15096−15097.
(30) Struthers, H., Spingler, B., Mindt, T. L., and Schibli, R. (2008) ″Click-to-Chelate″: Design and incorporation of triazole-containing metal-chelating systems into biomolecules of diagnostic and therapeutic interest. *Chem.—Eur. J. 14*, 6173−6183.
(31) Mindt, T. L., Mueller, C., Melis, M., deJong, M., and Schibli, R. (2008) ″Click-to-Chelate″: In vitro and in vivo comparison of a Tc-99m(CO)(3)-labeled N(tau)-histidine folate derivative with its isostructural, clicked 1,2,3-triazole analogue. *Bioconjugate Chem. 19*, 1689−1695.
(32) Mindt, T. L., Schweinsberg, C., Brans, L., Hagenbach, A., Abram, U., Tourwe, D., Garcia-Garayoa, E., and Schibli, R. (2009) A click approach to structurally diverse conjugates containing a central di-1,2,3-triazole metal chelate. *ChemMedChem 4*, 529−539.
(33) Mendelsohn, J., and Baselga, J. (2000) The EGF receptor family as targets for cancer therapy. *Oncogene 19*, 6550−6565.
(34) Paez, J. G., Janne, P. A., Lee, J. C., Tracy, S., Greulich, H., Gabriel, S., Herman, P., Kaye, F. J., Lindeman, N., Boggon, T. J., Naoki, K., Sasaki, H., Fujii, Y., Eck, M. J., Sellers, W. R., Johnson, B. E., and Meyerson, M. (2004) EGFR mutations in lung cancer: Correlation with clinical response to gefitinib therapy. *Science 304*, 1497−1500.
(35) Zhang, H. T., Berezov, A., Wang, Q., Zhang, G., Drebin, J., Murali, R., and Greene, M. I. (2007) ErbB receptors: from oncogenes to targeted cancer therapies. *J. Clin. Invest. 117*, 2051−2058.
(36) Roengvoraphoj, M., Tsongalis, G. J., Dragnev, K. H., and Rigas, J. R. (2013) Epidermal growth factor receptor tyrosine kinase inhibitors as initial therapy for non-small cell lung cancer: Focus on epidermal growth factor receptor mutation testing and mutation-positive patients. *Cancer Treat. Rev. 39*, 839−850.
(37) Master, A. M., and Sen Gupta, A. (2012) EGF receptor-targeted nanocarriers for enhanced cancer treatment. *Nanomedicine 7*, 1895−1906.
(38) Cohen, S. (1962) Isolation of a mouse submaxillary gland protein accelerating incisor eruption and eyelid opening in new-born animal. *J. Biol. Chem. 237*, 1555−1562.
(39) Bhirde, A. A., Patel, V., Gavard, J., Zhang, G. F., Sousa, A. A., Masedunskas, A., Leapman, R. D., Weigert, R., Gutkind, J. S., and Rusling, J. F. (2009) Targeted killing of cancer cells in vivo and in vitro with EGF-directed carbon nanotube-based drug delivery. *ACS Nano 3*, 307−316.
(40) Patra, C. R., Bhattacharya, R., Wang, E. F., Katarya, A., Lau, J. S., Dutta, S., Muders, M., Wang, S. F., Buhrow, S. A., Safgren, S. L., Yaszemski, M. J., Reid, J. M., Ames, M. M., Mukherjee, P., and Mukbopadhyay, D. (2008) Targeted delivery of gemcitabine to pancreatic adenocarcinoma using cetuximab as a targeting agent. *Cancer Res. 68*, 1970−1978.
(41) Saki, M., Toulany, M., Sihver, W., Zenker, M., Heldt, J. M., Mosch, B., Pietzsch, H.-J., Baumann, M., Steinbach, J., and Rodemann, H. P. (2012) Cellular and molecular properties of Y-90-labeled cetuximab in combination with radiotherapy on human tumor cells in vitro. *Strahlenther. Onkol. 188*, 823−832.
(42) Yang, L. L., Mao, H., Wang, Y. A., Cao, Z. H., Peng, X. H., Wang, X. X., Duan, H. W., Ni, C. C., Yuan, Q. G., Adams, G., Smith, M. Q., Wood, W. C., Gao, X. H., and Nie, S. M. (2009) Single chain epidermal growth factor receptor antibody conjugated nanoparticles for in vivo tumor targeting and imaging. *Small 5*, 235−243.
(43) Nordberg, E., Friedman, M., Gostring, L., Adams, G. P., Brismar, H., Nilsson, F. Y., Stahl, S., Glimelius, B., and Carlsson, J. (2007) Cellular studies of binding, internalization and retention of a radiolabeled EGFR-binding affibody molecule. *Nucl. Med. Biol. 34*, 609−618.
(44) Sexton, K., Tichauer, K., Samkoe, K. S., Gunn, J., Hoopes, P. J., and Pogue, B. W. (2013) Fluorescent affibody peptide penetration in glioma margin is superior to full antibody. *PLoS One 8*, e60390.
(45) Roovers, R. C., van Dongen, G., and Henegouwen, P. (2007) Nanobodies in therapeutic applications. *Curr. Opin. Mol. Ther. 9*, 327−335.
(46) Huang, L., Gainkam, L. O. T., Caveliers, V., Vanhove, C., Keyaerts, M., De Baetselier, P., Bossuyt, A., Revets, H., and Lahoutte, T. (2008) SPECT imaging with (99m)Tc-labeled EGFR-specific nanobody for in vivo monitoring of EGFR expression. *Mol. Imaging Biol. 10*, 167−175.
(47) Zarschler, K., Witecy, S., Kapplusch, F., Foerster, C., and Stephan, H. (2013) High-yield production of functional soluble single-domain antibodies in the cytoplasm of *Escherichia coli*. *Microb. Cell Fact. 13*, 12:97.

(48) Vaneycken, I., D'Huyvetter, M., Hernot, S., De Vos, J., Xavier, C., Devoogdt, N., Caveliers, V., and Lahoutte, T. (2011) Immuno-imaging using nanobodies. *Curr. Opin. Biotechnol. 22*, 877−881.
(49) De Vos, J., Devoogdt, N., Lahoutte, T., and Muyldermans, S. (2013) Camelid single-domain antibody-fragment engineering for (pre)clinical in vivo molecular imaging applications: adjusting the bullet to its target. *Expert Opin. Biol. Ther. 13*, 1149−1160.
(50) Bell, A., Wang, Z. J., Arbabi-Ghahroudi, M., Chang, T. A., Durocher, Y., Trojahn, U., Baardsnes, J., Jaramillo, M. L., Li, S., Baral, T. N., O'Connor-McCourt, M., MacKenzie, R., and Zhang, J. B. (2010) Differential tumor-targeting abilities of three single-domain antibody formats. *Cancer Lett. 289*, 81−90.
(51) Gainkam, L. O., Huang, L., Caveliers, V., Keyaerts, M., Hernot, S., Vaneycken, I., Vanhove, C., Revets, H., De Baetselier, P., and Lahoutte, T. (2008) Comparison of the biodistribution and tumor targeting of two 99mTc-labeled anti-EGFR nanobodies in mice, using pinhole SPECT/micro-CT. *J. Nucl. Med. 49*, 788−795.
(52) Roovers, R. C., Laeremans, T., Huang, L., De Taeye, S., Verkleij, A. J., Revets, H., De Haard, H. J., and Vanbergenen Henegouwen, P. M. (2007) Efficient inhibition of EGFR signaling and of tumour growth by antagonistic anti-EFGR Nanobodies. *Cancer Immunol. Immunother. 56*, 303−317.
(53) Gainkam, L. O., Keyaerts, M., Caveliers, V., Devoogdt, N., Vanhove, C., Van Grunsven, L., Muyldermans, S., and Lahoutte, T. (2011) Correlation between epidermal growth factor receptor-specific nanobody uptake and tumor burden: a tool for noninvasive monitoring of tumor response to therapy. *Mol. Imaging Biol. 13*, 940−948.
(54) Li, Z. H., Zhao, R. J., Wu, X. H., Sun, Y., Yao, M., Li, J. J., Xu, X. H., and Gu, J. R. (2005) Identification and characterization of a novel peptide ligand of epidermal growth factor receptor for targeted delivery of therapeutics. *FASEB J. 19*, 1978−1985.
(55) Song, S. X., Liu, D., Peng, J. L., Sun, Y., Li, Z. H., Gu, J. R., and Xu, Y. H. (2008) Peptide ligand-mediated liposome distribution and targeting to EGFR expressing tumor in vivo. *Int. J. Pharm. 363*, 155−161.
(56) Mickler, F. M., Mockl, L., Ruthardt, N., Ogris, M., Wagner, E., and Brauchle, C. (2012) Tuning nanoparticle uptake: Live-cell imaging reveals two distinct endocytosis mechanisms mediated by natural and artificial EGFR targeting ligand. *Nano Lett. 12*, 3417−3423.
(57) Ongarora, B. G., Fontenot, K. R., Hu, X. K., Sehgal, I., Satyanarayana-Jois, S. D., and Vicente, D. G. H. (2012) Phthalocyanine-peptide conjugates for epidermal growth factor receptor targeting. *J. Med. Chem. 55*, 3725−3738.
(58) Han, C. Y., Yue, L. L., Tai, L. Y., Zhou, L., Li, X. Y., Xing, G. H., Yang, X. G., Sun, M. S., and Pan, W. S. (2013) A novel small peptide as an epidermal growth factor receptor targeting ligand for nanodelivery in vitro. *Int. J. Nanomed. 8*, 1541−1549.
(59) Addison, A. W., Rao, T. N., Reedijk, J., Rijn, J., and van Verschoor, G. C. (1984) Synthesis, structure, and spectroscopic properties of copper(II) compounds containing nitrogen/sulphur donor ligands; the crystal and molecular structure of aqua[1,7-bis(N-methylbenzimidazol-2-yl)-2,6- dithiaheptane]copper(II) perchlorate. *Dalton Trans. 7*, 1349−1356.
(60) Schwindinger, W. F., Fawcett, T. G., Lalancette, R. A., Potenza, J. A., and Schugar, H. J. (1980) Molecular structure of dichloro(1,4,7-triazacyclononane)copper(II), a macrocyclic triamine complex with an unusually small formation constant. *Inorg. Chem. 19*, 1379−1381.
(61) Kawamoto, T., Sato, J. D., Le, A., Polikoff, J., Sato, G. H., and Mendelsohn, J. (1983) Growth-stimulation of A431 cells by epidermal growth-factor − Identification of high-affinity receptors for epidermal growth factor by an anti-receptor monoclonal-antibody. *Proc. Natl. Acad. Sci. U.S.A. 80*, 1337−1341.
(62) Macdonald, J. L., and Pike, L. J. (2008) Heterogeneity in EGF-binding affinities arises from negative cooperativity in an aggregating system. *Proc. Natl. Acad. Sci. U.S.A. 105*, 112−117.
(63) Alvarado, D., Klein, D. E., and Lemmon, M. A. (2010) Structural basis for negative cooperativity in growth factor binding to an EGF receptor. *Cell 142*, 568−579.
(64) Downward, J., Parker, P., and Waterfield, M. D. (1984) Autophosphorylation sites on the epidermal growth-factor receptor. *Nature 311*, 483−485.
(65) Margolis, B., Rhee, S. G., Felder, S., Mervic, M., Lyall, R., Levitzki, A., Ullrich, A., Zilberstein, A., and Schlessinger, J. (1989) EGF induces tyrosine phosphorylation of phospholipase C-II-A potential mechanism for EGF receptor signaling. *Cell 57*, 1101−1107.
(66) Winograd-Katz, S. E., and Levitzki, A. (2006) Cisplatin induces PKB/Akt activation and p3(MAPK) phosphorylation of the EGF receptor. *Oncogene 25*, 7381−7390.
(67) Emlet, D. R., Moscatello, D. K., Ludlow, L. B., and Wong, A. J. (1997) Subsets of epidermal growth factor receptors during activation and endocytosis. *J. Biol. Chem. 272*, 4079−4086.
(68) Murphy, L. O., and Blenis, J. (2006) MAPK signal specificity: the right place at the right time. *Trends Biochem. Sci. 31*, 268−275.
(69) Schlessinger, J. (2002) Ligand-induced, receptor-mediated dimerization and activation of EGF receptor. *Cell 110*, 669−672.
(70) Ferguson, K. M., Berger, M. B., Mendrola, J. M., Cho, H. S., Leahy, D. J., and Lemmon, M. A. (2003) EGF activates its receptor by removing interactions that autoinhibit ectodomain dimerization. *Mol. Cell 11*, 507−517.
(71) Endres, N. F., Das, R., Smith, A. W., Arkhipov, A., Kovacs, E., Huang, Y. J., Pelton, J. G., Shan, Y. B., Shaw, D. E., Wemmer, D. E., Groves, J. T., and Kuriyan, J. (2013) Conformational coupling across the plasma membrane in activation of the EGF receptor. *Cell 152*, 543−556.
(72) Xue, F., Fang, J., Delker, S. L., Li, H., Martásek, P., Roman, L. J., Poulos, T. L., and Silverman, R. B. (2011) Symmetric double-headed aminopyridines, a novel strategy for potent and membrane-permeable inhibitors of neuronal nitric oxide synthase. *J. Med. Chem. 54*, 2039−2048.
(73) Kimura, S., Bill, E., Bothe, E., Weyhermüller, T., and Wieghardt, K. (2001) Phenylthiyl radical complexes of gallium(III), iron(III), and cobalt(III) and comparison with their phenoxyl analogues. *J. Am. Chem. Soc. 123*, 6025−6039.
(74) Sheldrick, G. M.; Schneider, T. R. (1997) SHELXL: High-resolution refinement, In *Macromolecular Crystallography, Part B, Volume 277* (Carter, C. W., Sweet, R. M., Eds.) pp 319−343, Academic Press.
(75) Azevedo, J. R., and Johnson, D. A. (1990) Temperature-dependent lateral and transverse-distribution of the epidermal growth-factor receptor in A431 plasma-membranes. *J. Membr. Biol. 118*, 215−224.
(76) Laemmli, U. K. (1970) Cleavage of structural proteins during assembly of head of bacteriophage-T4. *Nature 227*, 680−685.
(77) Costes, S. V., Daelemans, D., Cho, E. H., Dobbin, Z., Pavlakis, G., and Lockett, S. (2004) Automatic and quantitative measurement of protein-protein colocalization in live cells. *Biophys. J. 86*, 3993−4003.
(78) Manders, E. M. M., Verbeek, F. J., and Aten, J. A. (1993) Measurement of co-localisation of objects in dual-colour confocal images. *J. Microsc. 169*, 375−382.
(79) Scatchard, G. (1949) The attractions of proteins for small molecules and ions. *Ann. N.Y. Acad. Sci. 51*, 660−672.